Novel Uniform Asymptotic Solutions for Scattered Fields by an Impedance Circular Cylinder

Teruhiko Ida* and Toyohiko Ishihara*
* Department of Communication Engineering, National Defense Academy,
Hashirimizu, Yokosuka, 239-8686 Japan, E-mail : ishihara@cc.nda.ac.jp

I. Introduction

The studies on the scattering by an impedance circular cylinder with a radius of curvature sufficiently larger than the wavelength have been an important research subject for a variety of applications in the area of antennas and propagation [1]-[7].

In the present study, we shall derive a novel uniform GTD(extended UTD) solution for the scattered field by an impedance circular cylinder. The extended UTD solution, derived by applying the higher-order asymptotic formulas for the cylindrical functions, can be applied in the wide area extending from the transition region near the shadow boundary to the deep shadow region where the current UTD solution [4]~[6],[8] becomes increasingly inaccurate with the increasing frequency. We shall also derive the modified UTD solution from the new generalized Pekeris carot function by applying the residue theorem. The modified UTD solution is the improved version of the current UTD and the GTD and can be applied uniformly from the transition region in the lit region to the deep shadow region including the region near the impedance cylinder.

The validity of the extended UTD and the modified UTD is confirmed by comparing with the exact solution obtained from the eigenfunction expansion.

II. Uniform Asymptotic Solutions

2.1 Formulation and integral representation

Fig.1 shows the impedance circular cylinder with the radius of curvature $\boldsymbol{a}$, and the cylindrical coordinate system (ρ, ϕ, z) and the cartesian coordinate system (x, y, z). When the impedance cylinder is illuminated by an incident wave radiated from a line source $Q(\rho_0, \phi_0)$, the frequency-domain scattered field observed at the point $P(\rho, \phi)$ can be represented by the eigenfunction expansion. Then using the usual Watson transform, the eigenfunction solution is transformed into a integral representation as follows.

$$u_z^d = -\frac{i}{8}\int_{-\infty}^{\infty} \frac{H_\nu^{(2)\prime}(ka) + i\bar{C}H_\nu^{(2)}(ka)}{H_\nu^{(1)\prime}(ka) + i\bar{C}H_\nu^{(1)}(ka)} H_\nu^{(1)}(k\rho_0)H_\nu^{(1)}(k\rho)\exp(i\nu|\phi - \phi_0|)d\nu \tag{1}$$

$$\bar{C} = 1/Z_s \ \ (\mathrm{E-mode\ case}) \ , \ \ \bar{C} = Z_s \ \ (\mathrm{H-mode\ case}) \tag{1a}$$

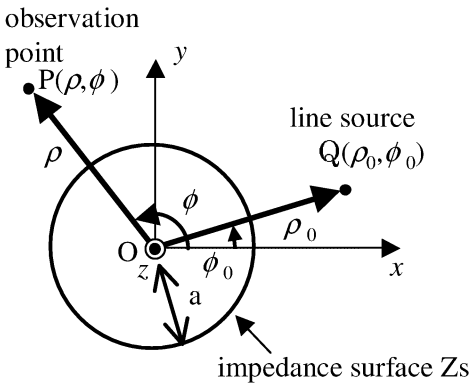

Fig.1 Impedance circular cylinder with the radius of curvature a and the normalized surface impedance Zs.

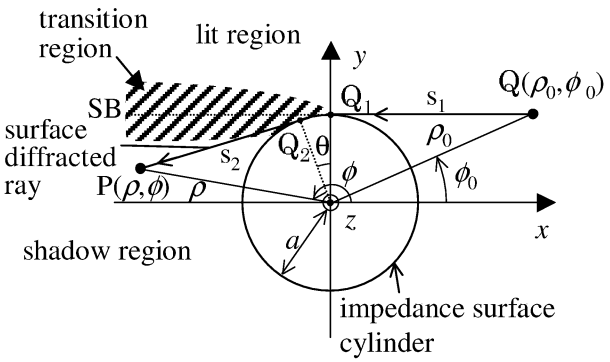

Fig.2 Shadow boundary(SB), transition region, and scattering phenomena.

ISBN: 4-88552-206-4 C3055©IEICE

where u_z^d denotes either the scattered electric field E_z^d(E-mode) or the scattered magnetic field H_z^d(H-mode), Z_s the normalized surface impedance of the cylinder. The time factor $\exp(-i\omega t)$ is suppressed. Eq.(1) describes only the scattered field excited by the incident wave on the impedance cylinder from the counterclockwise direction without circulating around the cylinder. Various scattered field representations are derived from (1) in the following sections.

2.2. Extended UTD solution in the transition region near the SB

Fig.2 shows the shadow boundary(SB), the transition region near the SB, and the scattering phenomena by the impedance cylinder. When the observation point $P(\rho,\phi)$ is located in the transition region near the SB, the Debye's approximation:

$$H_\nu^{(1)}(kx) \sim (2/\pi)^{1/2}\{(kx)^2-\nu^2\}^{-1/4}\exp\Big[i\{\sqrt{(kx)^2-\nu^2}-\nu\cos^{-1}\frac{\nu}{kx}\}-i\frac{\pi}{4}\Big] \tag{2}$$

for the Hankel functions $H_\nu^{(1)}(k\rho_0)$ and $H_\nu^{(1)}(k\rho)$, and the Airy function approximations:

$$\begin{aligned} H_\nu^{(1),(2)\prime}(ka) &\sim -(ka/2)^{-2/3}w_{1,2}'(t),\ \ \nu = ka+Mt,\ \ M=(ka/2)^{1/3}, \\ w_{1,2}'(t) &= Ai'(t)\mp iBi'(t) \end{aligned} \tag{3}$$

for the Hankel functions $H_\nu^{(1),(2)\prime}(ka)$ are applied in (1). Then by performing the straightforward analysis one may derive the following extended UTD solution.

$$u_z^d \sim u_{z,in}(Q_1)\exp(ik\ell)I(\xi,L)\exp(iks_2)/\sqrt{s_2} \tag{4}$$

$$u_{z,in}(Q_1) = \exp(iks_1+i\pi/4)/\sqrt{8\pi ks_1},\ \ s_1=\sqrt{\rho_0^2-a^2},\ \ s_2=\sqrt{\rho^2-a^2} \tag{5}$$

$$\ell = a\theta,\ \ \theta = |\phi-\phi_0|-\cos^{-1}(a/\rho_0)-\cos^{-1}(a/\rho) \tag{6}$$

where the integral $I(\xi,L)$ is given by

$$I(\xi,L) = B(k)\big[-\frac{\exp(i\pi/4)}{2\sqrt{\pi}\xi}F(X)+p_{s,h}^e(\xi,L)\big],\ \ B(k)=-M\sqrt{2/k}, \tag{7}$$

$$F(X) = -2iX\exp(-iX^2)\int_X^\infty \exp(i\tau^2)d\tau,\ \ X=\sqrt{2kL}\,\theta/2, \tag{8}$$

$$\begin{aligned} p_{s,h}^e(\xi,L) &= \frac{\exp(-i\pi/4)}{2\sqrt{\pi}}\int_{i\infty}^0 \frac{w_2'(t)-q_{s,h}w_2(t)}{w_1'(t)-q_{s,h}w_1(t)}\exp(i\xi t+i\frac{M^2}{2kL}t^2)dt \\ &+ \frac{\exp(-i\pi/4)}{\sqrt{\pi}}\int_0^\infty \frac{Ai'(t)-q_{s,h}Ai(t)}{w_1'(t)-q_{s,h}w_1(t)}\exp(i\xi t+i\frac{M^2}{2kL}t^2)dt, \end{aligned} \tag{9}$$

$$\xi = M\theta,\ \ L=s_1s_2/(s_1+s_2)\ \ ,q_s=iM/Z_s\ \ (\mathrm{E-mode})\ \ ,\ \ q_h=iMZ_s\ \ (\mathrm{H-mode}). \tag{10}$$

The computation time and the accuracy of the numerical integration of the generalized Pekeris function $p_{s,h}^e(\xi,L)$ in (9) are the same as those for the computation of the conventional Pekeris function applied in the UTD [8] .

It will be shown in Sec. III that the extended UTD in (4) can be applied in the wide area including the deep shadow region near the impedance cylinder with the large ka value.

2.3. Modified UTD solution

The integral representation $I(\xi,L)$ in (7) expressing the scattering phenomena occurring along the arc of the impedance circular cylinder may be represented by

$$I(\xi,L) = B(k)\frac{\exp(-i\pi/4)}{2\sqrt{\pi}}\int_{C_o}\frac{w_2'(t)-q_{s,h}w_2(t)}{w_1'(t)-q_{s,h}w_1(t)}\exp(i\xi t+i\frac{M^2}{2kL}t^2)dt \tag{11a}$$

$$= B(k)\frac{\exp(-i\pi/4)}{\sqrt{\pi}}\int_{Co}\frac{Ai'(t)-q_{s,h}Ai(t)}{w_1'(t)-q_{s,h}w_1(t)}\exp(i\xi t+i\frac{M^2}{2kL}t^2)dt = \hat{P}_{s,h}(\xi,L), \tag{11b}$$

where the integration contour C_o is running along the positive imaginary axis from $i\infty$ to 0 and then along the positive real axis from 0 to ∞ in the complex t-plane. The new generalized Pekeris carot function $\hat{P}_{s,h}(\xi, L)$ in (11b) can be evaluated rigorously by applying the residue theorem. Substituting the residue series solution into (4) and performing the straightforward manipulation yield the following modified UTD solution

$$u_z^d \sim u_{z,in}(Q_1)\{\sum_{m=1}^{\infty} D_m(Q_1)A_m(Q_1)\exp(ik\ell - \Omega_m\ell)D_m(Q_2)A_m(Q_2)\}G(ks_2) \tag{12}$$

where $D_m(Q_{1,2})$ denotes the surface diffraction coefficient at the diffraction point $Q_{1,2}$(see Fig.2), Ω_m the attenuation coefficient of the creeping wave propagating along the arc of the impedance cylinder from the diffraction point Q_1 to Q_2, and $A_m(Q_{1,2})$ is the new coefficient which modifies the conventional GTD's diffraction coefficient $D_m(Q_{1,2})$. Those coefficients corresponding to the H-mode case are defined as follows:

$$D_m(Q_{1,2}) = (2M/\sigma_m)^{1/2}/\{Ai'(-q_m)\sqrt{g_m}\},\ \ \Omega_m = M\sigma_m^{-1}\exp(-i\pi/6), \tag{13}$$

$$A_m(Q_{1,2}) = \exp\{M^2\sigma_m^2\exp(i7\pi/6)/(2ks_{1,2})\},\ \ g_m = 1 - q_h\{\frac{w_1'(t_m)}{t_m w_1(t_m)}\}. \tag{14}$$

The eigenvalues $\sigma_m (m = 1, 2, 3\cdots)$ and the corresponding t_m are obtained from the following characteristic equation [4],[9]

$$Ai'(-\sigma_m) - \exp(-i\frac{\pi}{6})Z'MAi(-\sigma_m) = 0,\ \ t_m = \sigma_m\exp(i\pi/3). \tag{15}$$

The coefficients $D_m(Q_{1,2})$, Ω_m, and $A_m(Q_{1,2})$ for the E-mode case are defined in similar manner.

We will show that, in Section III, the modified UTD solution in (12) can be applied even in the illuminated side of the transition region and in the deep shadow region where the current UTD solution [5],[6] deviates substantially from the exact eigenfunction solution.

2.4. Extended UTD solution in the transition region in the illuminated region

When the observation point is located in the illuminated region in the transition region, the creeping angle θ defined by (6) takes the negative value(see Fig.2). Then by substituting $\theta = -|\theta|$ and $\xi = \hat{\xi} = -|\xi| = -M|\theta|$ into (4), one may derive the following extended UTD solution which can be applied in the illuminated region.

$$u_z^d \sim u_{z,go} + \hat{u}_z^d\ ,\ \ u_{z,go} \doteqdot \exp(ikL_0 + i\pi/4)/\sqrt{8\pi kL_0} \tag{16}$$

$$\hat{u}_z^d = u_{z,in}(Q_1)\exp(-ika|\theta|)I(\hat{\xi}, L)\exp(iks_2)/\sqrt{s_2} \tag{17}$$

$$I(\hat{\xi}, L) = B(k)\Big[-\frac{\exp(i\pi/4)}{2\sqrt{\pi}\hat{\xi}}F(\hat{X}) + p^e(\hat{\xi}, L)\Big],\ \ \hat{X} = \sqrt{2kL}|\theta|/2,\ \ \hat{\xi} = -M|\theta| \tag{18}$$

where $u_{z,go}$ defined in (16) denotes the direct geometrical ray radiated from the source Q and reaching the observation point P. The distance from Q to P is L_o.

III. Numerical Results and Discussions

In this section, we perform the numerical calculations required to assess the validity and the utility of the various asymptotic solutions derived in the previous section. Only the typical results are presented in Figs.3 and 4 since all of the relevant solutions apply to the other parameters with the accuracy similar to those shown here.

In Fig.3, the electric field magnitude curves(E-mode) are calculated as the function of the azimuthal distance $|\phi - \phi_0|$. The parameters used in the calculations are $ka = 78.0$, $a = 10.0$, $\rho_0 = 150.0$, $\rho = 90.0$, and $\varepsilon = 8.0$, σ(conductivity)$= 1.0$. The source and observation points are located far away from the impedance cylinder. The SB is located at $|\phi - \phi_0| = 169°$ in this calculation. The extended UTD(- - -) in (4), the modified UTD(∘) in (12), the conventional

UTD(-▲-) [5],[6] , and the geometrical optics(GO) agree excellently in the respective regions with the exact solution(—) calculated from the eigenfunction expansion.

In Fig.4, the E-mode electric field magnitude curves observed near the impedance cylinder are calculated as the function of $|\phi - \phi_0|$. The numerical parameters $ka = 78.0$, $a = 10.0$, $\rho_0 = 15.0$, $\rho = 12.0$, and $\varepsilon = 8.0$, $\sigma = 1.0$ are used in the calculations. The extended UTD and the modified UTD agree very well with the exact solution, while the conventional UTD becomes increasingly inaccurate as the observation point moves toward the deep shadow region, i.e., as $|\phi - \phi_0|$ increases in the shadow region. It is interesting to note that the modified UTD in (12) agrees every well with the exact solution even in the illuminated region near the SB.

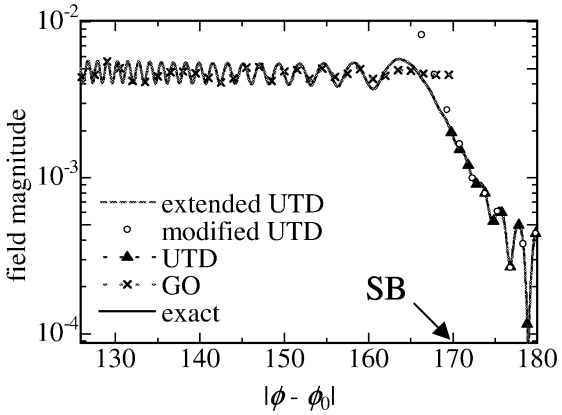

Fig.3 Comparison of asymptotic solutions with the exact solution for the observation point located far from the impedance cylinder.

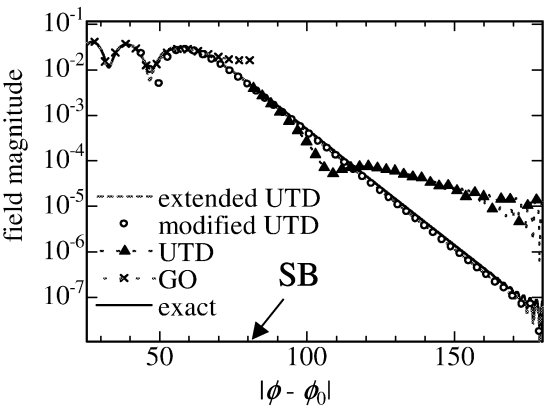

Fig.4 Comparison of asymptotic solutions with the exact solution for the observation point located near the impedance cylinder.

V. Conclusion

In this paper, by applying the higher-order asymptotic formulas for the Hankel functions, we have derived the novel extended UTD and modified UTD solutions for the scattered fields by the impedance circular cylinder. The validity and the physical interpretation of the uniform asymptotic solutions are confirmed by comparing with the exact solution calculated from the eigenfunction expansion.

References

[1] J. R. Wait and A. M. Conda, "Patteren of an antenna on a curved lossy surface," IEEE Trans. Antennas and Propag., Vol. AP-6, pp.348-359, Oct. 1958.

[2] N. A. Logan, "General research in diffraction theory," Vols.1 and 2, Lockheed Missiles and Space Div. Rep. LMSD-288087 and LMSD-288088, 1959.

[3] V. A. Fock, Electromagnetic Diffraction and Propagation Problems, Oxford, Pergamon, 1965.

[4] N. Wang, "Electromagnetic scattering from a dielectric coated circular cylinder," IEEE Trans. Antennas and Propag., Vol. AP-33, No.9, pp.960-963, Sept. 1985.

[5] H. Kim and N. Wang, "UTD solution for electromagnetic scattering by a circular cylinder with thin lossy coatings," IEEE Trans. Antennas and Propag., Vol. AP-37, No.11, pp.1463-1472, Nov. 1989.

[6] H. H. Syed and J. L. Volakis, "High-frequency scattering by a smooth coated cylinder simulated with generalized impedance boundary conditions," Radio Science, Vol.26, No.5, pp.1305-1314, Sep.-Oct. 1991.

[7] A. V. Osipov, H. Kobayashi, and K. Hongo, "Shadow boundary currents in the problem of high-frequency electromagnetic diffraction by a circular impedance cylinder," IEICE Trans, Vol.E-21-C, No.10, pp.1655-1666, Oct. 1998.

[8] P. H. Pathak, "An asymptotic analysis of the scattering of plane waves by a smooth convex cylinder," Radio Science, Vol.14, No.3, pp.419-435, May-June 1979.

[9] Teruhiko Ida and Toyohiko Ishihara, "Time-domain asymptotic solutions in the transition regions near geometrical boundaries and near caustics for scattering by a dielectric cylinder," 2003 IEEE Antennas & Propagation Society International Symposium, Ohio, USA, Vol.4, pp.840-843, June 2003.